Journal of Applied and Natural Science
14(4), 1272 - 1285 (2022)
ISSN : 0974-9411 (Print), 2231-5209 (Online)
journals.ansfoundation.org

Research Article

Vertical characteristics of precipitating cloud systems during different phases of life cycle of cloud systems using satellite-based radar over tropical oceanic areas

Shailendra Kumar*
Space Physical Laboratory, Vikram Sarabhai Space Centre, Trivandrum (Kerala), India
Shweta Srivastava
Department of Mathematics, SRM AP University, Amravati (Andhra Pradesh), India

*Corresponding author. Email: shailendrak89@gmail.com

Article Info
https://doi.org/10.31018/jans.v14i4.3691
Received: July 7, 2022
Revised: November 8, 2022
Accepted: November 15, 2022

How to Cite
Kumar, S. and Srivastava, S. (2022). Vertical characteristics of precipitating cloud systems during different phases of life cycle of cloud systems using satellite-based radar over tropical oceanic areas. *Journal of Applied and Natural Science*, 14(4), 1272 - 1285. https://doi.org/10.31018/jans.v14i4.3691

Abstract
An index-based approach is applied to investigate the climatology of precipitating cloud systems (PCSs) during different phases of evolution over twelve tropical oceanic areas using Precipitation Radar (PR) onboard at the satellite. In the present study, a Precipitating cloud system (PCS) is defined as the connecting pixels having radar reflectivity (Z_e) ≥ 17 dBZ using composite Z_e field. The three-dimensional structure of PCS is observed using all the PR beams contributing to horizontal PCS pixels. An average vertical profile is drawn and then converted it into the liquid water content using the relation $M=3.44 \times Z^{(4/7)} \times 10^{(-6)}$ (where M is in gm^{-3} and Z is in $mm^6\ m^{-3}$). A dimensionless ratio, namely, the ratio for maturity levels (RMLs) is defined by dividing the normalized cloud liquid water at 4 km to 2 km for each PCSs. These RMLs values are used to classify the PCSs into different phases of development. Further the PCSs are also divided with (RML<0.75) and without bright band (BB, RML≥ 0.75), which indicates the latter phase of cloud evolution. The results reveal that initial stage PCSs have higher Z_e at higher vertical level, and once the bright band is observed, Z_e decreases rapidly above the BB. Regional differences have similar trends in Z_e profiles during different RMLs. Similar average vertical profiles over different tropical areas lead to that understanding the microphysics of PCSs in one area could use in other areas too. The convective precipitation area dominates during the initial stage and decreases as the PCSs mature. This is the first time the TRMM data is used to investigate the evolution of PCSs using the indexing approach.

Keywords: Bright band, Convective precipitation, Life-cycle of MCS, Stratiform precipitation TRMM PR, Vertical profile of reflectivity

INTRODUCTION

Mesoscale Convective Systems (MCSs) transport mass, water, and momentum from lower atmosphere level to higher levels and play a vital role in tropical radiative budget (Del Genio *et al*., 2005). They are also important for Earth's water cycle as they produce most of the accumulated rainfall (Roca *et al.,* 2014; Kumar *et al.*, 2019a). Global Atlantic Research Program Atlantic Tropical Experiment (GATE, 1974) supplied the first understanding of MCS (Houze and Betts, 1981). Byers and Braham (1949) used airborne data to investigate the life cycle of MCSs and mainly divided them into phases, namely the initial, mature and dissipating phase.

The present study uses Tropical Rainfall Measuring Mission Precipitation Radar (TRMM-PR) data to study the climatology of precipitating cloud systems (PCSs) over tropical oceanic areas. The life span of a majority of MCSs is from a few to several hours (Houze and Betts, 1981; Houze, 1989) and the TRMM revisit time is at least several hours. In view of this, the only TRMM data are not suitable for the study of the life cycle of MCSs. On the other hand, the features of the attenuated corrected radar reflectivity factor (Z_e) field that characterize the different phases of an MCS life cycle may be exploited to study the spatial variations in MCS properties (Houze, 1982, Kumar and Bhat, 2019). For example, the formative and intensifying stages mainly consist of convective cells, and a melting band is absent while intense/tall Cumulonimbus clouds (Cbs) along with a bright band (BB) are present in the mature

phase (Houze and Betts, 1981; Kumar 2017a;b; Kumar *et al*., 2020a). In the dissipating stage, fraction of active Cb clouds are small and a melting band is prominently present (Houze and Chang 1977; Houze, 1982). Relative are of Z_e filed also varies in convective and stratiform precipitation (Houze and Betts, 1981; Houze, 1989; Kumar and Bhat, 2019; Kumar *et al*., 2020a).

Historically, geostationary Infrared observations were used to investigate life cycle of MCSs (Chen and Houze, 1997; Machado *et al*., 1998; Mathon and Laurent, 2001). Now a days, scientists are frequently combining the, ground-based radar, geostationary satellite and TRMM sensors to extract the properties of MCSs (Kondo *et al.,* 2006; Futyan and Del Genio, 2007; Cetrone and Houze, 2009; Imaoka and Nakamura, 2012; Bhat and Kumar, 2015; Kumar *et al*., 2020a). For example, Futyan and Genio (2007) compared the life cycle of MCS over Africa and Latin America by combining the TRMM-PR and TRMM Lightning Imaging Sensor (LIS) sensors using a cloud tracking algorithm They observed the fundamental differences within the life cycle over land and oceans. Cetrone and Houze (2009) combined the TRMM-PR, CloudSat cloud profiling radar (CPR) and ground-based radar to investigate anvil clouds over Bay of Bengal, the Maritime Continent, and West Africa. Imaoka and Nakamura (2012) investigated the life cycle properties of tropical cold cloud systems using ground-based radar, namely *Multifunctional Transport Satellite-1R* (MTSAT-1R) and TRMM-PR data. They divided the life cycle of cloud clusters into 1h to 5h durations and observed the vertical profiles of convective and stratiform rainfall within the different phases of evolution. Convective and stratiform precipitation fraction area is an indication of the evolution of cloud systems, and TRMM-PR based observation shows the compatible convective stratiform statistics with various airborne and ground-based radar data (Schumacher and Houze, 2000; Heymsfield *et al.,* 2010).

TRMM-PR provides the Z_e data and could be very useful to see the climatology and regional differences in the PCS on a global basis. Not much information is available during different phases of evolution over different tropical oceanic regimes. The present study aims to fill this gap. One of the main objectives is to draw a climatological vertical profile of the Ze during different phases of life cycle over tropical oceanic areas. It will help us quantify which tropical ocean regimes have intense rainfall during particular phases. So, the present study explored the vertical characteristics of PCSs over various tropical oceanic areas during different states of evolution, which are proxy for the life cycle of MCS. The TRMM-PR provides data around the globe, and the total data size is very huge. So, carrying the analysis over the entire globe is a huge task, and thus twelve oceanic areas were considered here to investigate the vertical characteristics of PCSs during different phases of evolution.

MATERIALS AND METHODS

Data

TRMM-PR is the first space borne precipitation radar operated since December 1997 (Kummerow *et al.,* 1998). The PR operates at 13.8 GHz (2.2 cm wavelength, K*u* band), with the horizontal and vertical resolution of ~5 km ´ ~5 km and 0.25 km, respectively. The swath width of PR increased from 215 km to 247 km in August 2001, as its height was increased from 350 km to 402.5 km. TRMM-PR consists of 49 beams, each separated by 0.71°, and the extreme beams make an angle of 17° with the central beam (25th beam). Here the present study used TRMM 2A25 data, whose primary product is Z_e in dBZ and derived as Z_e (dBZ) =10´log(Z) where Z is in mm^{6}m^{-3}. It is very important to know that TRMM PR does not provide the actual height, but the distance at each 0.25 km along each PR beam starts from the Earth's Ellipsoid. The present study has corrected the altitude information for each PR beam and algorithm is well described in Bhat and Kumar (2015); Kumar and Bhat, (2015, 2016). Also, TRMM 2A23 data is used for convective and stratiform rain classification (Awaka *et al.,* 2009). TRMM data is used for 15 years of period from 1998 to 2014. The present study also used the National Centers for Environmental Prediction (NCEP, Kalnay *et al.,* 1996) data at 2.5°´2.5° grid resolution, for sea surface temperature (SST), temperature and specific humidity profiles for same period. The present study selected twelve oceanic areas over tropical oceans, based on SST derived from NCEP data (Fig. 1). The twelve oceanic areas (Fig. 1) are the climatological the warmest SSTs in the JJAS (June-July-August-September) and JFM (January -February-March) months (Kumar and Bhat, 2016). SST was chosen because it is well documented that it largely influences deep convection (Graham and Barnett, 1987; Waliser and Graham, 1993; Sherwood *et al.,* 2004).

Precipitating cloud systems (PCS), three dimensional vertical PCS (3DCVS)

The definition of PCS and 3DCVS are briefly explained in Kumar (2016) and discussed briefly here also. For identifying PCSs, it is essential to fix a Z_e threshold at some reference height from radar echoes (Roca *et al.,* 2017). Since TRMM-PR provides the three-dimensional field of Z_e, the present study first projected the maximum Z_e from all the PR levels. A PCS is defined as an area of the connected pixels with $Z_e \geq 17$ dBZ in X-Y directions as well as along the diagonal direction (Kumar *et al.,* 2019b; Kumar *et al.,* 2020b) in the maximum projection. PCSs containing at least one radar

pixel of Ze>40 dBZ were considered here for study as they represented strong convective echoes (Kumar and Silva, 2019;2020). Fig. 2 shows an example of PCS captured over Myanmar regimes by TRMM PR. The color bar in dBZ unit shows the intense precipitation areas (Ze≥40 dBZ), followed by the weaker radar Z_e. Fig. 3 shows an example of the three-dimension vertical structure (3DCVS) of PCS. 3DCVS contains the vertical extension of PR beams over the area of a PCS. The number along the x-axis refers to individual PR within the PR swath area. The present study arranged the TRMM PR beams based on their echo-base height. The echo-base height is defined based on the first occurrence of 17 dBZ (minimum detectable signal from PR, Li and Schumacher, 2011). Within the population of the cloud systems, small cloud systems could contribute to a higher number, but their contribution in total rainfall is much less (Kumar *et al.,* 2019b; Kumar *et al.,* 2020b). Thus, the present study set a minimum PCSs area for further analysis. Only PCSs were considered, which had a minimum area of 200 km^2 and the PCSs where at least 5% TRMM PR beams must cross the 4 km altitude within PCS to avoid too shallow clouds (Kumar and Bhat, 2017; Kumar, 2018).

Method of analysis

Radar reflectivity is calculated considering the hydrometeors in liquid phase (Houze, 1993) in the radar data. In general, the single polarized radar provides the Z_e, which is purely interpreted as cloud property, and understands as the condensed water per unit volume (Houze, 1993). This is the basis of Z-R relationship, which does not include the radar characteristics. So, Z_e was converted in the physical space of CLW using the relation $M=3.44´Z^{(4/7)}´10^{(-6)}$ (where M is in gm^{-3} and Z is in mm^6 m$^{-3)}$ (Greene and Clark, 1972). The area of PCSs varies from 200 km^2 to more than 25000 km^2 among selected areas, so the absolute average CLW may be affected by the number of cloudy pixels. To minimize the effect of the size of PCSs, normalized CLW (NCLW) was defined for each PCSs. NCLW is calculated by dividing the CLW at each PR vertical level by the highest CLW at any PR level, which was used to identify the maturity levels (e.g., RMLs). Convective rain rate keeps increasing towards the Earth surface from rain top to a very low level (2-3 km), and stratiform rain rate a peak around the freezing level (~4.5 km) (Liu and Fu, 2001). NCLW had peaks either above or below the 3 km altitude (not shown). Based on NCLW, peak altitude RML was defined.

RML = Maximum NCLW (4-6 km)/Maximum NCLW (1-3 km) Eq. 1

Fig. 4 shows the RMLs distribution within the selected areas. Here the lower (upper) edge of box showed the 25 (75) percentiles, whereas the red line showed the median value. Bay of Bengal (R-1) and Maritime Continent (R-4) showed the highest median value of RML (0.9) during June to September (JJAS) months and January to March (JFM) months, respectively e.g. most matured PCSs. Central Pacific Ocean (R-6) and Atlantic Ocean (B-5) showed the least RML during JJAS and JFM months.

Fig. 5 shows the vertical cross-section for various RMLs. The left-hand panels showed the projection of maximum Z_e on the surface, whereas the right side showed the corresponding composite vertical profiles. It will help us to visualize the RMLs. For example, RML1 PCSs were quite small and discrete. The Z_e val-

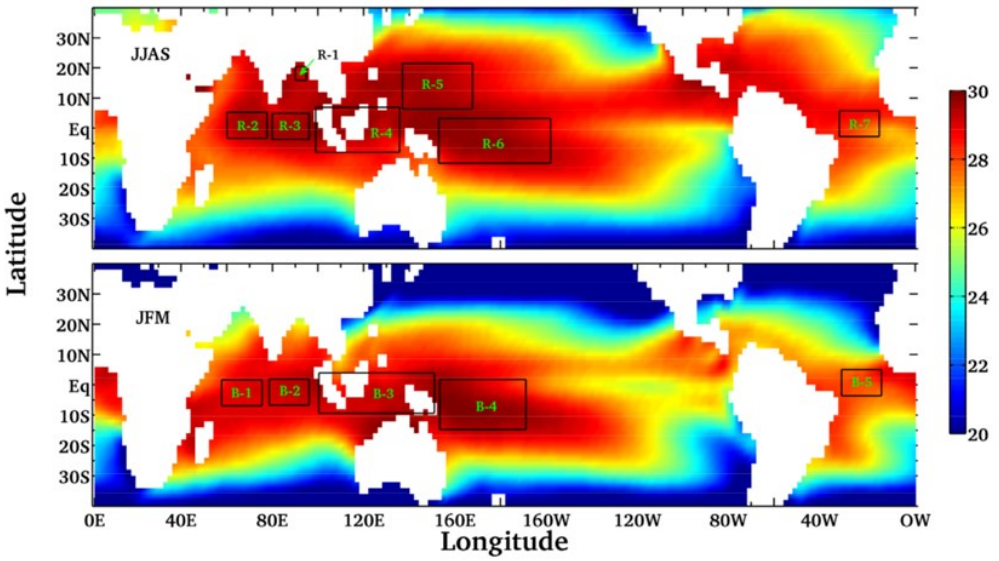

Fig. 1. *SST over the ten-year period from 2001 to 2010. NCEP reanalysis SSTs products are shown. Upper row shows the climatological SST for the months between June to September, whereas lower row shows the climatological SST for the months between January to march months. Areas selected for detailed analysis are shown by rectangular boxes. Colorbar shows the sea surface temperature in* °C

ues in the PCS core are not very high and end up between 35-40 dBZ. RML2 PCS showed that PCS core Z_e was higher than 40 dBZ up to 6-8 km altitude and few PR beams were crossing 15 km altitude, too, although the BB is absent in the vertical structure. RML3 PCS showed the weak signature of BB (scan number, 6030-6040) with trailing stratiform clouds (scan number, 5960-5990). It could correspond to mature phase of PCSs. RML4 PCSs have a strong BB (scan number 2940-3000) and stratiform clouds trailing the individual deep cloud cells, with the highest Ze value near the surface. The Vertical structure of RML3 and RML4 were nearly similar so the study chose an algorithm to separate the weak and strong BB.

Fig. 6 shows the average NCLW for various RMLs over the central Pacific Ocean. PCSs with RML <0.75 peak at 2 km while above 2 km, RML decreases with altitude. As PCSs mature, average NCLW increases with altitude, and attains highest magnitude for RML ≥1.0. Also, PCSs for RML >0.75 has a peak near the freezing level and indicate the existence of BB (Fig 5). The study separates the RML into four groups, which correspond to various RMLs during the life cycle of PCSs and classifies the PCSs with and without BB (as discussed earlier, Table 1). Fig. 7 shows the number of PCSs classified during different RMLs over different areas and most of the time PCSs are observed in RML3.

RESULTS

Nearly 50000 TRMM PR swaths are considered here to study the climatology of PCSs over various tropical oceanic areas.

Average profiles of radar reflectivity (Z_e) during various RMLs

Fig. 8 shows the average vertical profile of Z_e in PCSs for different RMLs. To reduce the confusion, only the extreme cases are labelled by thick and colored lines whereas the rest of the areas are shown by thin black lines. Average Z_e profiles show nearly similar vertical trends over different tropical oceanic areas, but average Z_e are different for different RMLs. RML1 and RML2 PCSs show a decrease in average Z_e towards the cloud top to cloud base. RML3 PCSs show the evolution of the BB as Z_e peaks near the freezing level. The strongest feature of BB is observed in RML4 PCSs and average Z_e is highest between 4-4.5 km, near to freezing level. During all the RML, average Z_e decreases above 4.5 km and regional differences are observed below 4.5 km. Average Z_e profiles show the RML1 and RML2 PCSs are more like the PCSs in initial stage as Z_e peaks near the surface (Leary and Houze, 1979), whereas RML3 and RML4 PCSs show a peak near freezing level and more like to mature and dissipating stage (Leary and Houze, 1979; Williams *et al.,* 1989).

Average vertical profiles show nearly similar average vertical profiles and similar evolution patterns in PCSs (Roca *et al.,* 2017) among various tropical oceanic regimes. During the initial stage (RML1 PCSs) the east equatorial Ocean (B-2), Central Pacific Ocean (B-4) and Atlantic Ocean (B-5) show the highest Z_e values whereas north Pacific Ocean (R-5) and Atlantic Ocean (R-7) shows the least values at all the PR levels. As the PCSs intensify (RML2 PCSs), Maritime Continent (R-4) and Atlantic Ocean (B-5) show the highest Z_e, whereas center Pacific (R-5) and Atlantic Ocean (R-7) have the least Z_e. During mature stage (RML3 PCSs), the Atlantic Ocean (B-5) and Bay of Bengal (R-1) have the higher Z_e whereas Central Pacific (R-5) has the least Z_e in average vertical profiles. In dissipating stage (RML4 PCSs) Bay of Bengal (R-1) has the highest Z_e at all the PR levels, whereas Equatorial Indian Ocean (B-1) and R-3 have the least Z_e. The regional differences are highest either in the initial stage or dissipating stage, and least in the mature stage.

Areal evolution of PCS during different RMLs

Fig. 9 shows the altitude evolution of 3DCVS during different M_{LS} using the Normalized Fraction Precipitation Area (NFPA) with altitude, which is an indication of the fractional area of the precipitation during different RML. NFPA is calculated by dividing the number of cloudy pixels (Z_e≥17) at each altitude by the maximum number of cloudy pixels at any altitude within each PCSs. RML1, RML2, and RML3 PCSs have the highest NFPA near 2 km and increase above 2 km as PCSs mature, and RML3 PCSs show a little tendency of higher NFPA at 4 km. On average, 50% of maximum NFPA

Table 1. Classification for different ratios of maturity levels (RMLs) corresponds to different stages of development. Corresponding stages of life of PCS for RMLs, are shown in the fourth column

S. No.	Ratio of maturity level (RML)	RML value	PCSs classification
1.	Maturity level-1 (RML1)	RML ≤0.5	Initial stage with no BB
2.	Maturity level-2 (RML2)	0.5< RML ≤ 0.75	Intensifying stage
3.	Maturity level-3 (RML3)	0.75< RML < 1.0	Mature stage with weak signature of BB
4.	Maturity level-4 (RML4)	RML ≥ 1.0	Dissipating stage with strong signature of BB

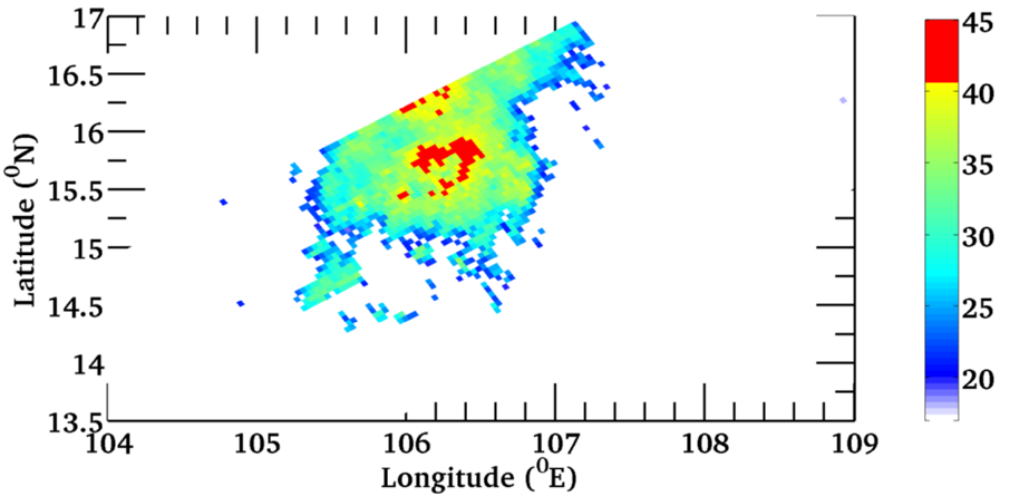

Fig. 2. *An example of a cloud system captured by the TRMM PR. Area of connected cloudy pixels with $Z_e \geq 17$ dBZ is considered as a cloud system. Color bar on the right shows the reflectivity value in dBZ*

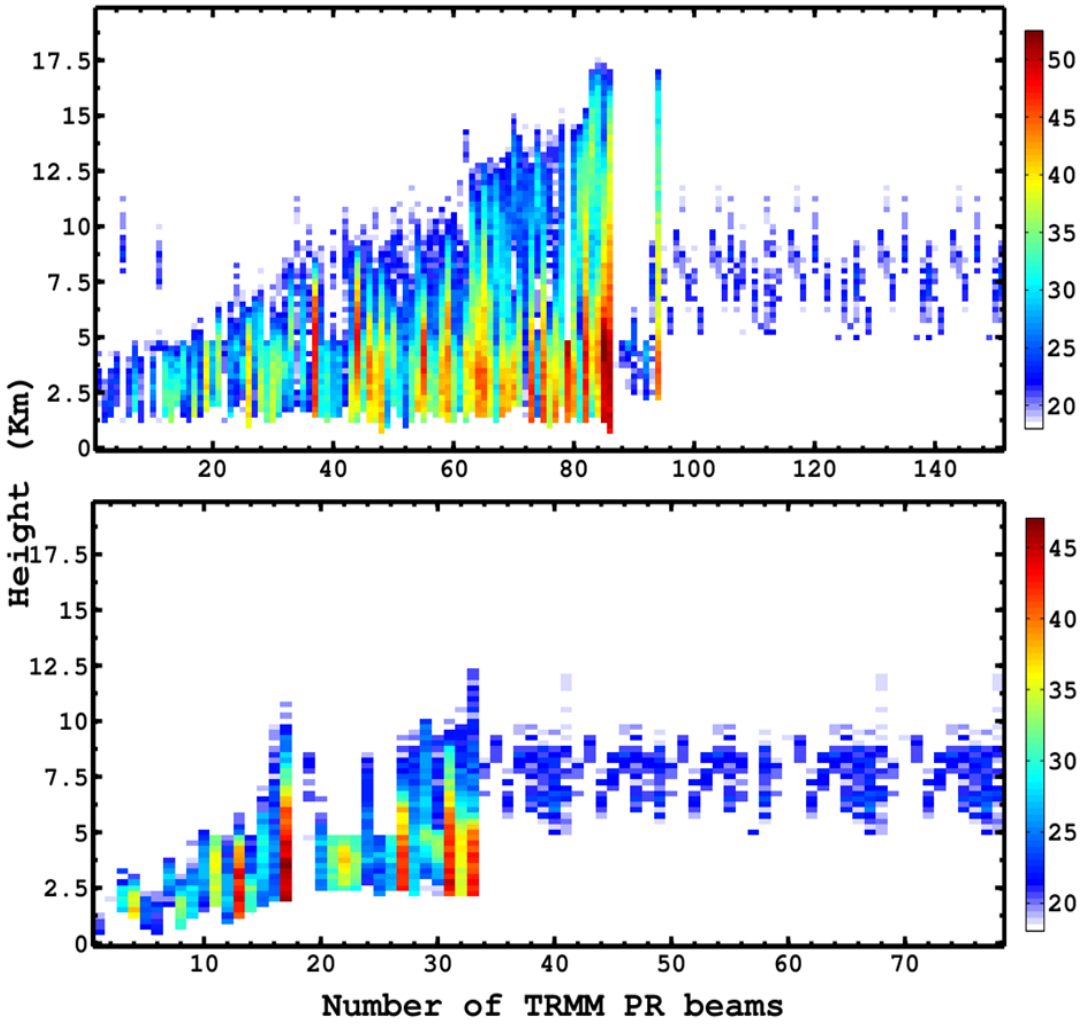

Fig. 3. *An example of three-dimensional vertical structure of cloud systems. Each TRMM-PR beam contribute to the cloud systems. Color bar on the right shows the reflectivity value in dBZ. Both the cloud systems show the TRMM-PR beams with echo-base height below the 2 km altitude and cross the 12 km and indicating the cumulonimbus clouds, whereas PR beams with echo-base height above the 5 km altitude are the part of anvil or stratiform precipitation*

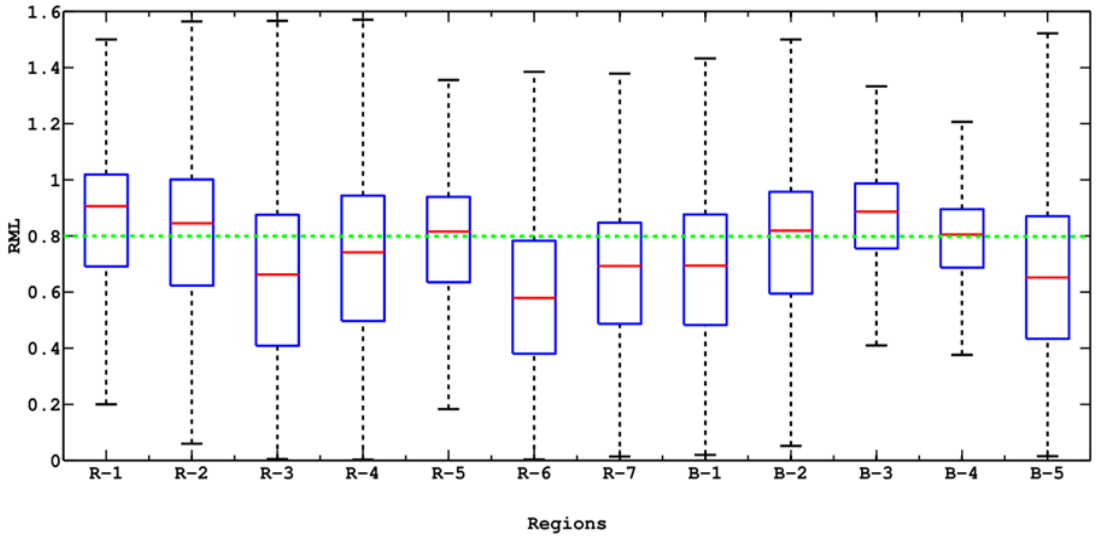

Fig. 4. *Variation of RML of PCSs over the different areas. For most areas, the median of the RML is near 0.8*

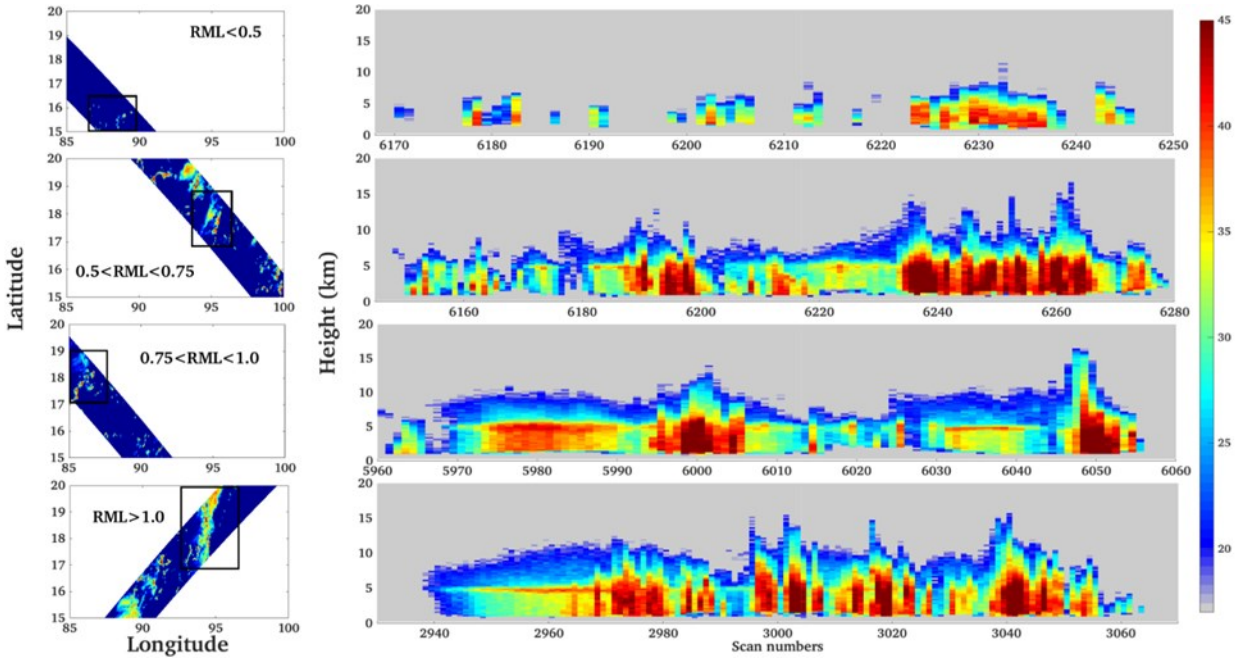

Fig. 5. An *example of vertical cross section of Z_e for different RML*

comes from below 3, 5, 6 and 6 km altitude as PCSs matures (RML1-RML4), whereas the corresponding height for 20% of NFPA is 5, 6.25, 8 and 8 km, respectively. Above 8 km, the NFPA does not show the much difference and could be because of the PR sensitivity as at higher altitudes is not able to distinguish between ice and liquid phase.

CFAD during different RMLs

Contoured frequency by altitude diagram (CFAD) summarizes the frequency distribution of Z_e (Yuter and Houze, 1995). Fig. 10a shows the CFADs during different RMLs and the dark red line shows the 5 km altitude, near to 0°C level (Houze *et al.,* 2007). Major differences occurred immediately above and below the 0° C level. CFADs below (above) the 0°C level showed the broad frequency distribution, indicating the high (low) probability of Z_e and intense (less intense) precipitation (Houze *et al.,* 2007). Below the 0°C, RML1 PCSs (initial/intensifying stage) showed the highest width of Z_e within 2.5-3 km with highest modal value of 20-25 dBZ. CFAD for RML2 PCSs showed similar characteristics, but lower Z_e ends at high altitude and corresponds to the intensifying stage (Fig. 10b). RML3 and RML4 PCSs showed higher probability either below & above and only above 5 km (depends on the area) and showed the signature of a BB as Z_e peak towards the right side near 5 km (Fig. 10c-d, Houze *et al.,* 2007), and indicates mature and dissipating stages.

Fig. 11 shows the convective to stratiform precipitation

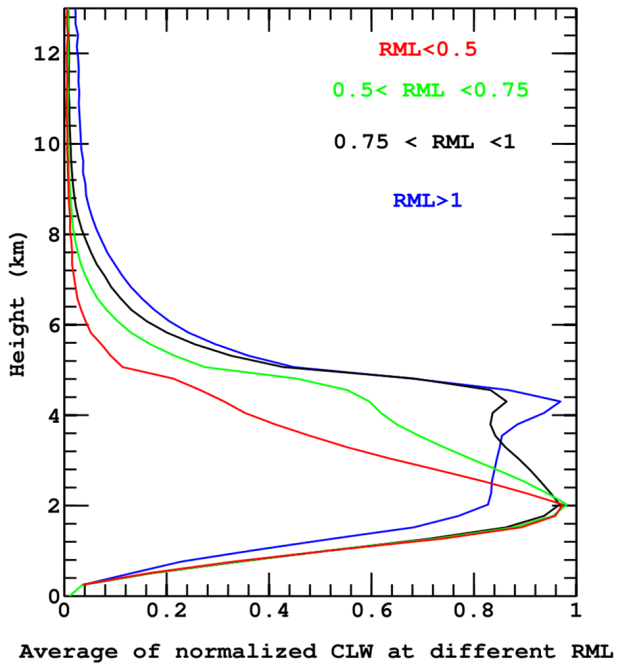

Fig. 6. *Average of normalized cloud liquid water for PCSs during different maturity levels. RML higher than 0.75 shows the increase in normalized average cloud liquid water near 4.5 km and coinciding with the freezing level, indicating the PCSs may be in the mature and dissipating stage, as evidenced by the bright band*

dissipating stage. All the areas show similar trends except over central Pacific Ocean (R-6).

DISCUSSION

In average vertical profiles (Fig. 8), Ze shows similar trends during different RMLs over different tropical oceanic areas. For example, during the initial and intensifying stage, Z_e was highest near the surface, whereas during dissipating stage, higher Z_e was observed near 0°C, which corresponded to different micro physical processes (Fig. 6 and 8). Z_e is the product of size and concentration of hydrometeors and proportional to the 6th power of the diameter of the hydrometeors (Houze, 1993). Cloud micro physics controlled the growth and removal of hydrometeors (e.g., Fabry and Zawadzki, 1995) and the vertical characteristics of Z_e depended on the balance between the growth and removal of hydrometeors during different stages of development. A strong updraft carried the condensed water and small droplets (either clouds or raindrops) at higher altitudes during the growing (initial) and intensifying stage. While going upward, the size of cloud droplets increased because of condensation and collision-coalescence mechanism below the freezing level (Fig. 8 ; Fig. 9, e.g., Houze, 1993; Kumar et al. 2020c). During the mature and dissipating stage, BB peaks were near the

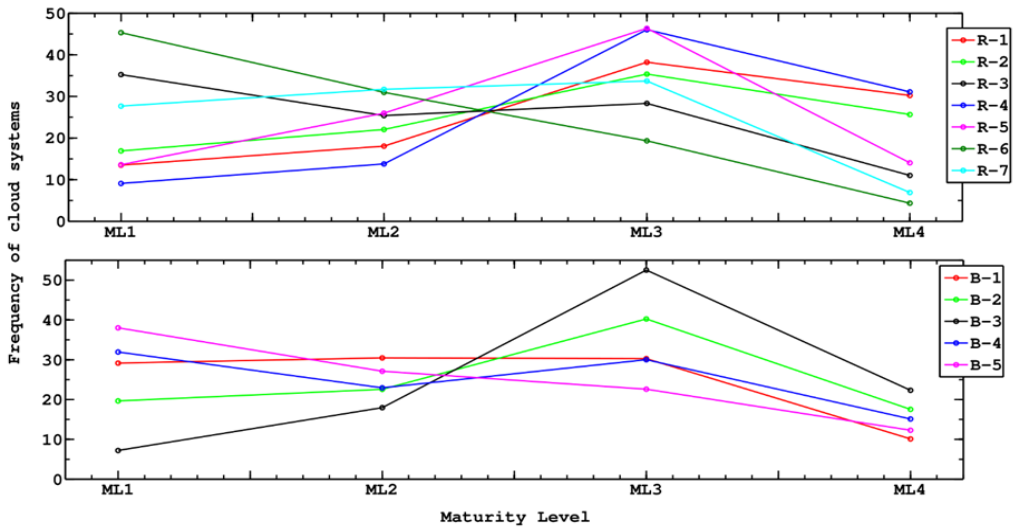

Fig. 7. *Frequency of occurrence of PCSs for different RML over different tropical oceanic areas*

ratio (CSR) calculated for different RMLs. CSR is the highest for RML1 PCSs and decreases as the PCSs mature. Highest CSR, e.g., the highest convective precipitation area for RML1 PCSs supports the argument that RM L1 corresponds to the early stage of development of PCSs (e.g., initial or growing stage). CSR is nearly ~0.5 (50%) for RML2 PCSs and higher than RML1 CSs. RML3 and RML4 PCSs have less convective precipitation area, while the latter has the highest stratiform precipitation area and shows the PCSs in freezing height (Fig. 8; Fig. 9) due to the melting of snow into water and able to produce higher hydrometeors because of the coating of water on melting snow or the higher fall velocity near the freezing height (Fig. 8; Houze, 1993). In short, the increasing tendency of Z_e near the surface in the initial stage could be because its size increased, whereas decreasing tendency of Z_e was because of the faster removal of hydrometeors (e.g., Beard and Pruppacher, 1969).

The present study also compared the CFADs from past

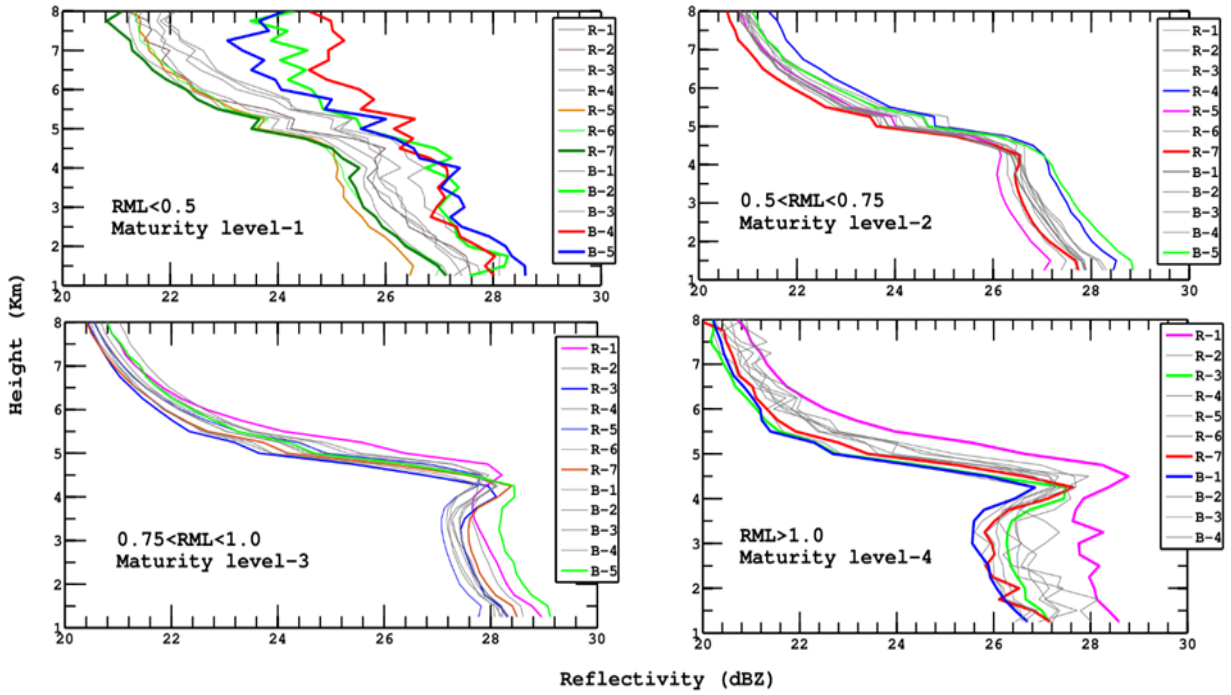

Fig. 8. *An example of average reflectivity profile of PCSs during different maturity levels (RMLs). Here extreme cases are shown by dark color line whereas rest of the cases are shown by thin black line. Average profile shows highest Ze values near 2 km in its early stages. Average vertical profiles showing the peak in reflectivity near 4 km fort the PCSs in mature and decaying stage*

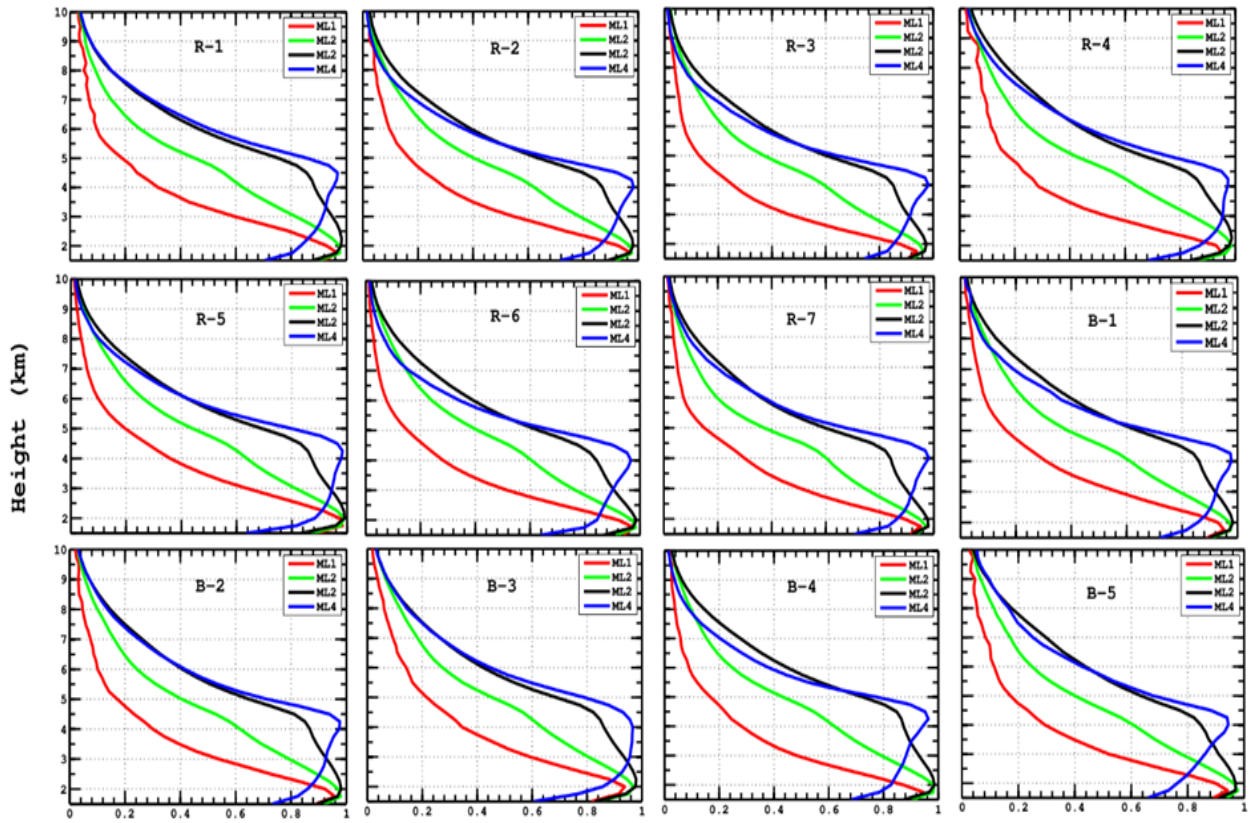

Fig. 9. *Areal evolution of fraction precipitation area for PCSs during different maturity levels. RML1, RML2 and RML3 PCSs have the highest fraction of precipitation area at 2 km and increases at higher altitude as cloud systems mature. RML4 PCSs have highest fractional precipitation area at 4 km*

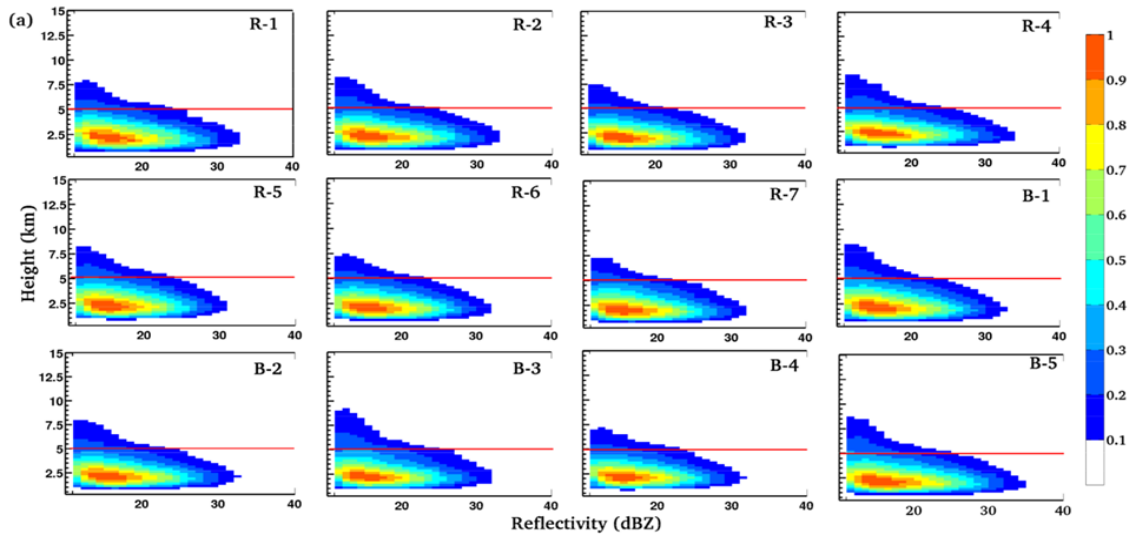

Fig. 10a. *Contoured frequency by altitude diagram (CFAD) of PCSs for RML <0.5 over different tropical oceanic areas. Colorbar on the right side shows the relative probability of occurrence of reflectivity*

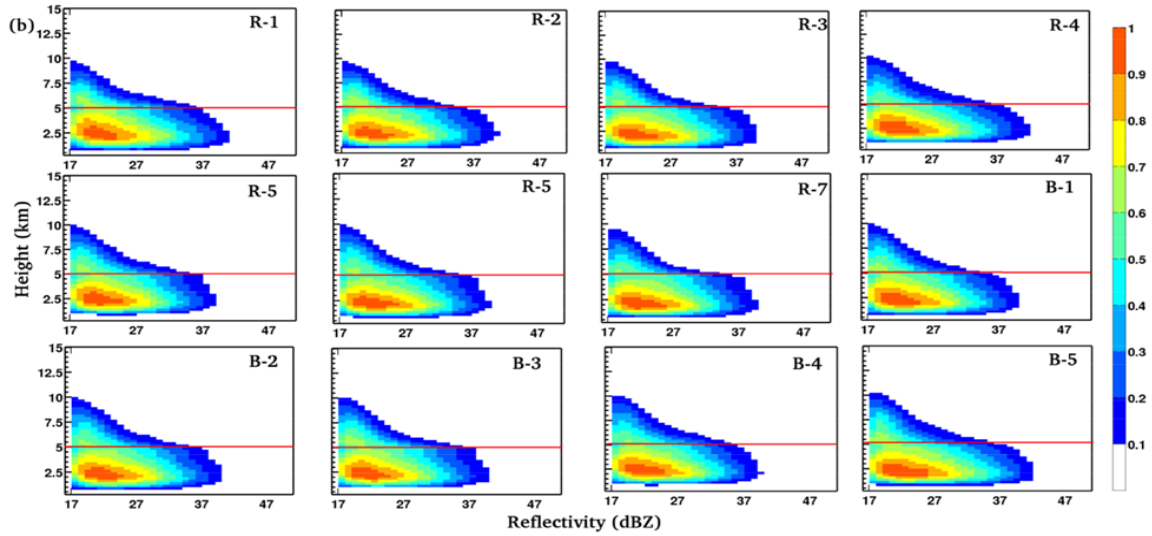

Fig. 10b. *CFAD of PCSs for 0.5< RML <0.75 over different tropical oceanic areas. Colorbar on the right side shows the relative probability of occurrence of reflectivity*

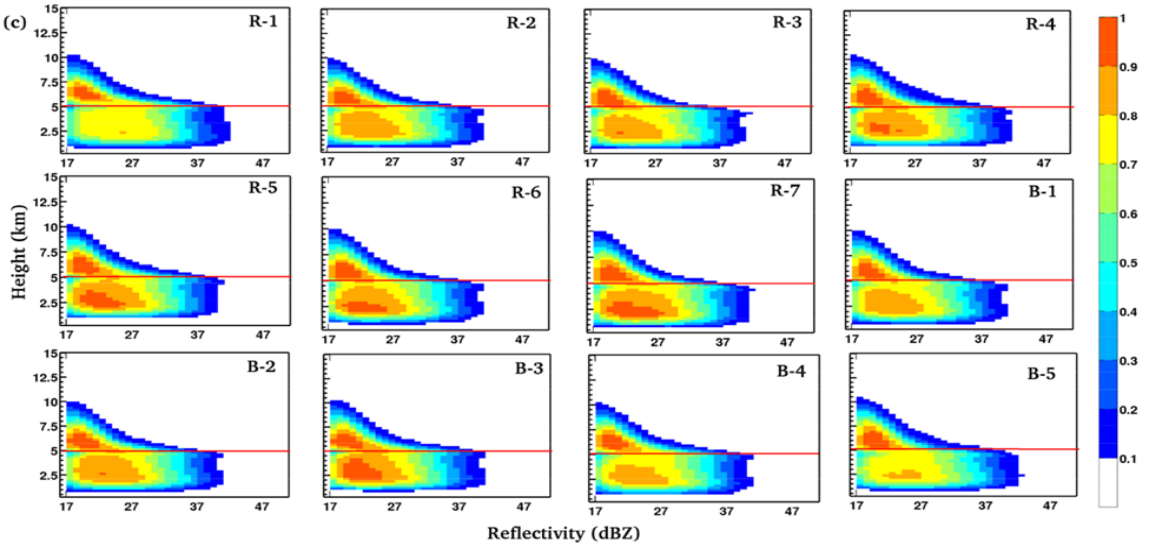

Fig. 10c. *CFAD of PCSs for 0.75 < RML <1.0 over different tropical oceanic areas. Colorbar on the right side shows the relative probability of occurrence of reflectivity*

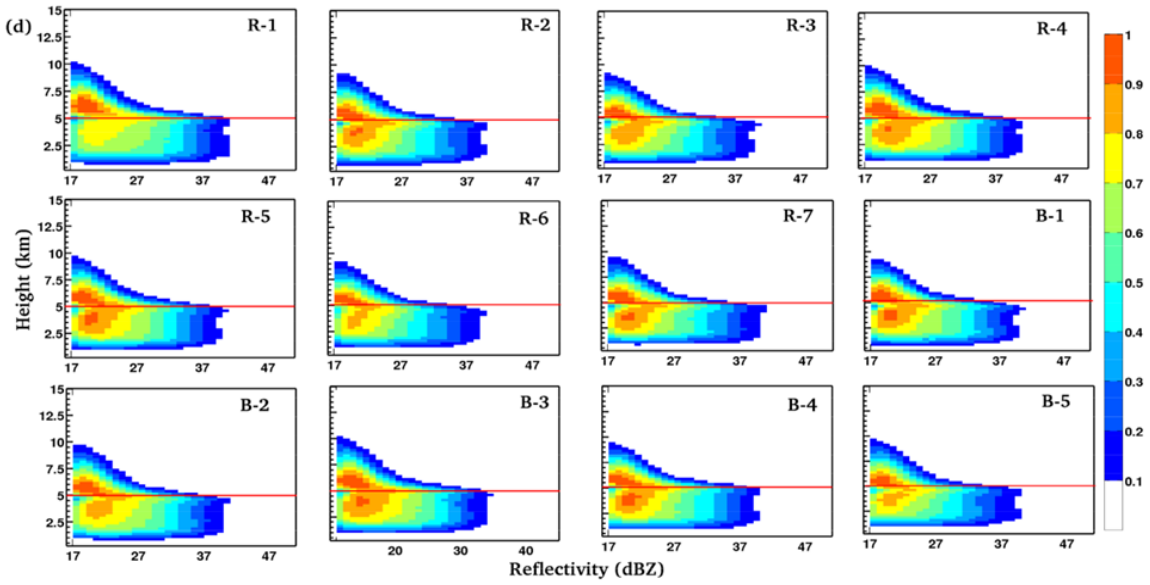

Fig. 10d. *CFAD of PCSs for RML > 1.0 over different tropical oceanic areas. Colorbar on the right side shows the relative probability of occurrence of reflectivity*

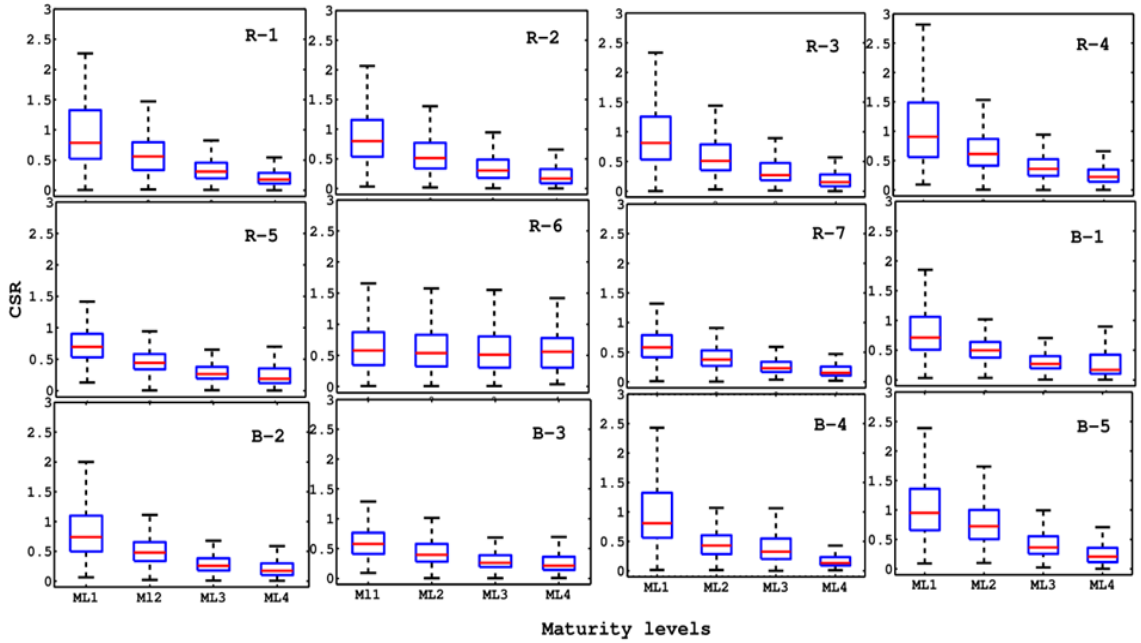

Fig. 11. *Convective to stratiform ratio (CSR) during different phases of evolution e.g. RML. Sequence is same as shown in Fig. 8 and 9*

studies in the literature with the CFADs presented here. Fig. 12 shows the CFADs for convective + stratiform precipitation (total reflectivity) for different M_{LS}, and broad feature indicates that RML1 and RML2 PCSs CFADs (Fig.12a-b) were more like convective CFADs, whereas RML3 and RML4 PCSs CFADs (Fig.11c-d) were more like stratiform CFADs. PCSs belonging to RML1 and RML2 showed the higher Z_e mode (38-42 dBZ) below 5 km, with decreasing trends at higher altitudes, like those in convective precipitation. CFADs for RML3 and RML4 PCSs (Fig. 12c-d) showed the Z_e peaks near 5 km, similar to those in stratiform precipitation, and Z_e width showed similar decreasing trends as those shown in stratiform precipitation.

Direct inter-comparisons are not possible with the past literature because of different algorithms used in various studies. Still, the CFADs, average profiles and PCSs area during different phases of evolution showed nearly similar features (Fig. 10 from Imaoka and Nakamura, 2012 and many more). It revealed that the methodology was able to capture the various phases of PCSs. For example, Futyan and Genio (2006) studied the life cycle properties of the cloud clusters using ground-based radar and TRMM data. A close similarity

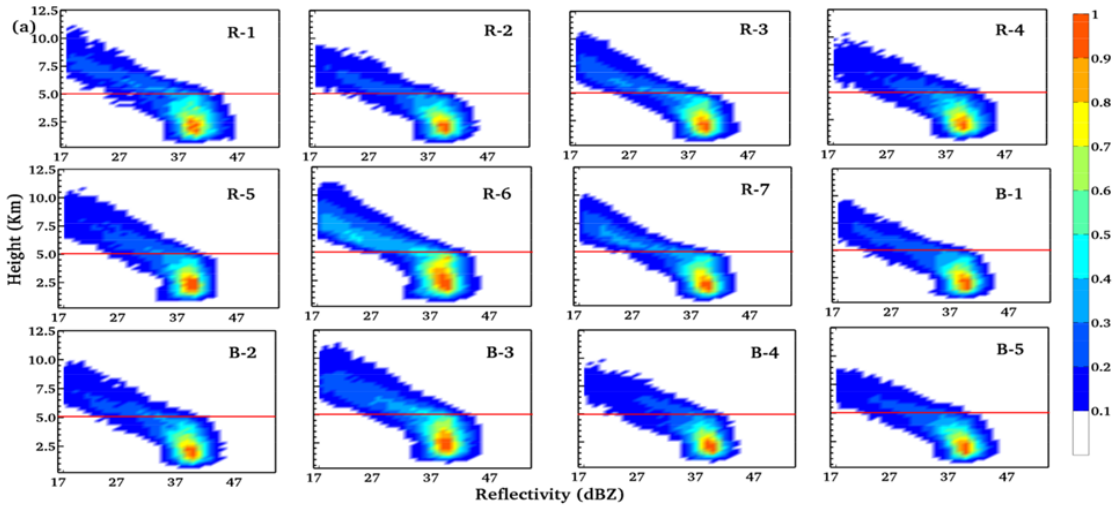

Fig. 12a. *CFAD for convective+stratiform precipitation for RML < 0.5 over different oceanic areas. Colorbar on the right side shows the relative probability of occurrence of reflectivity*

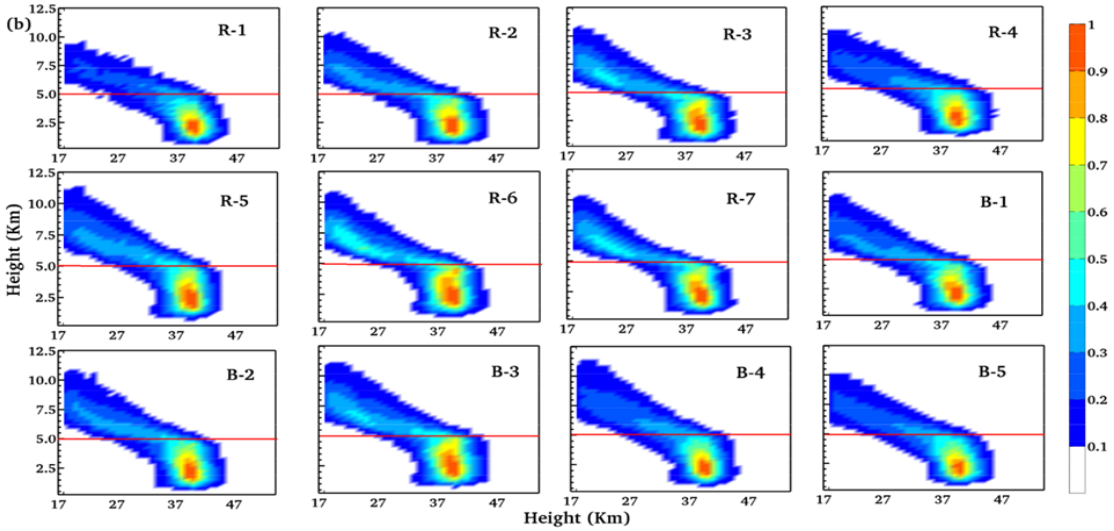

Fig. 12b. *CFADs for convective + stratiform precipitation for 0.5 < RML < 0.75 over different oceanic areas. Colorbar on the right side shows the relative probability of occurrence of reflectivity*

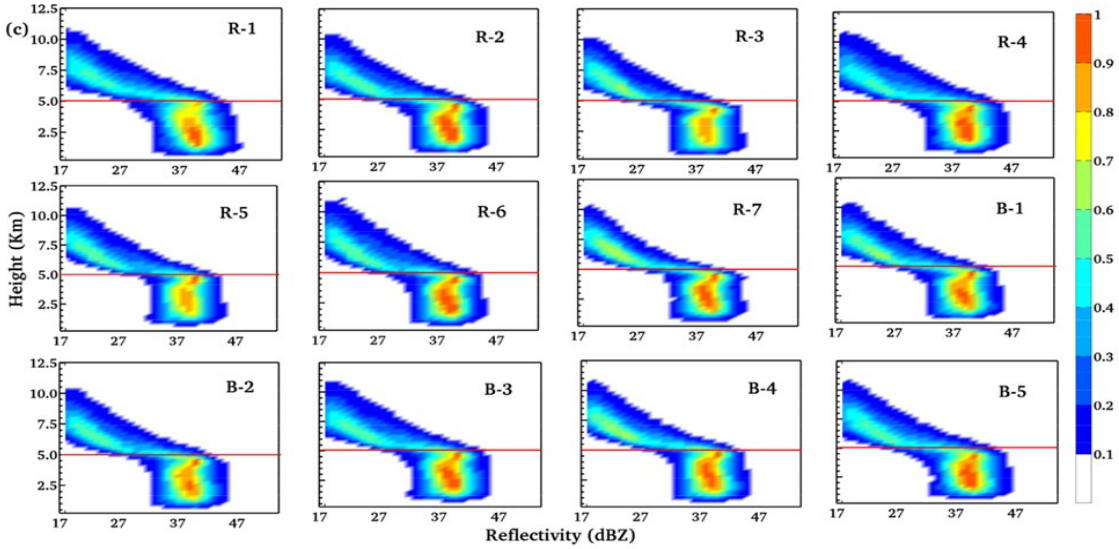

Fig. 12c. *CFADs for convective + stratiform precipitation for 0.75 < RML < 1.0 over different oceanic areas. Colorbar on the right side shows the relative probability of occurrence of reflectivity*

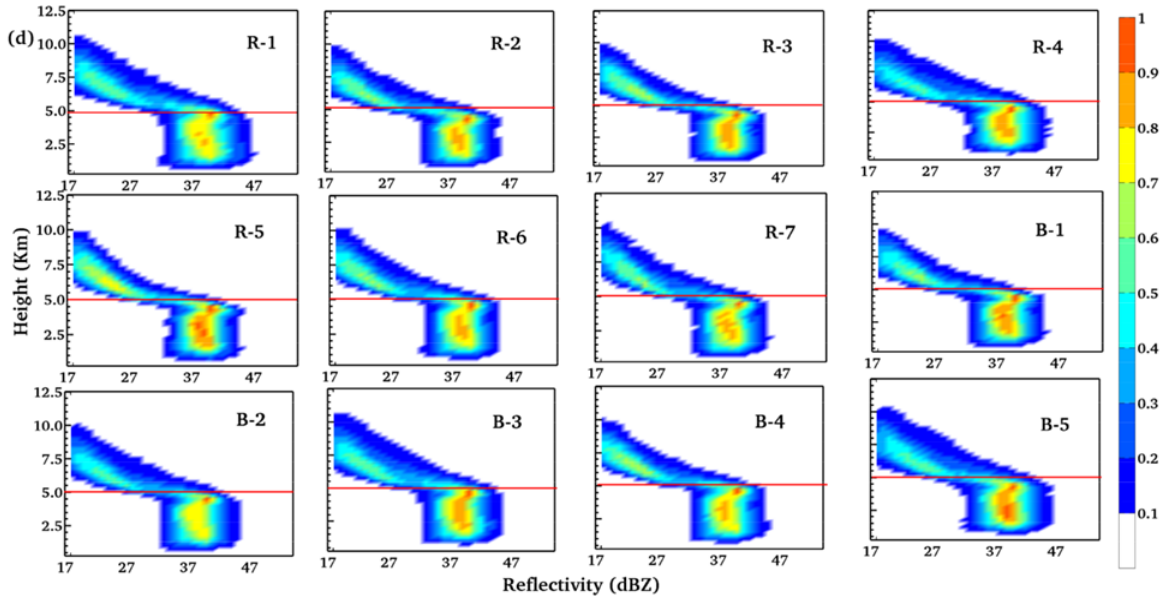

Fig. 12d. *CFADs for convective + stratiform precipitation for RML_D > 1.0 over different oceanic areas. Colorbar on the right side shows the relative probability of occurrence of reflectivity*

was observed in CFAD for the mature stage (Fig. 6 from Futyan and Genio, 2006) and RML3 PCSs. It is suggested that proposed methodology is able to capture the stage of development effectively over the Atlantic Ocean. Imaoka and Nakamura (2012) plotted the average vertical profiles for different phases of evolution and a close similarity was observed between the present and mentioned study. At the last, it is essential to mention that PR revisit time at the same locations in several days and is not able to track the cloud systems but using the index-based approach based on the vertical profiles of $Z_{e,}$ it was able to observe the climatology in the three-dimensional vertical structure of PCSs.

Conclusion

The major conclusions are as follows:

1.Average vertical profiles showed higher reflectivity values near the surface during the initial stage, whereas dissipating stage PCSs showed the peak in reflectivity near the freezing height.

2.The different chosen oceanic regimes showed the peak in reflectivity during different maturity levels and depended on the balance between growth and removal of hydrometeors during different maturity levels.

3.Higher regional differences in the reflectivity values were observed below the freezing level, and initial and dissipating phase PCSs have the highest regional differences.

4.Higher TRMM sensitivity could lead to fewer regional differences above the 8 km PR vertical levels as it could not detect the ice.

5.The climatology of the cloud vertical structures remained almost similar over all the tropical oceanic regimes. Average vertical profiles and CFAD did not vary widely over different tropical oceanic basins and understanding in one area could lead to other areas too.

6.The convective/stratiform ratio decreased as the cloud system matured and was minimum during the decaying stage.

From the present study, it is quite clear that the defined indexing approach is able to discriminate the PCSs into different phases of evolution. The different phases of evolution show the different vertical trends in Z_e. Although the different regions are leading similar vertical trends during different phases, it is suggested that understanding cloud systems over one tropical oceanic region can be expandable to other regions too. The present study could be very useful from the modelling perspective of view as the one can gain the better knowledge of the cloud's extension during different phases and predict them better in future.

Conflict of interest

The authors declare that they have no conflict of interest.

REFERENCES

1. Awaka, J., Iguchi, T. & Okamoto K. (2009). TRMM PR standard algorithm 2A23 and its performance on bright band detection. *Journal of Meteorological Society of Japan,* 87A, 31–52.
2. Bhat, G. S. & Kumar, S. (2015). Vertical structure of cumulonimbus towers and intense convective clouds over the South Asian region during the summer monsoon season. *Journal of Geophysics Research Atmosphere,* 120,

doi:10.1002/2014JD022552.
3. Beard, K. V. & Pruppacher, H. R. (1969). A determination of the terminal velocity and drag of small water drops by means of a wind tunnel. *Journal of Atmospheric Science*, 26, 1066 – 1072.
4. Byers, H. R. & Braham, R. R. (1949). The Thunderstorm: Report of the Thunderstorm Project, 287. U.S. Government Printing Office.
5. Chen, S. & Houze, R. A. (1997). Diurnal variation and life-cycle of deep convective systems over the tropical Pacific warm pool. *Quarterly Journal of Royal. Meteorological Society,* 123, 357–388.
6. Cetrone, J. & Houze, R. A. (2009). Anvil clouds of tropical mesoscale convective systems in monsoon regions. *Quarterly Journal of Royal Meteorological Society,* **135**, 305-317.
7. Del Genio, A. D., Kovari, W., Yao, M. S. & Jonas, J. (2005). Cumulus microphysics and climate sensitivity. *Journal of Climate*, 18, 2376–2387.
8. Fabry, F. & Zawadzki. I. (1995). Long-term Radar Observations of the Melting Layer of Precipitation and Their Interpretation. *Journal of the Atmospheric Sciences,* 52, 838–851.
9. Futyan, J. M. & Del Genio, A. D. (2007). Deep convective system evolution over Africa and the tropical Atlantic. *Journal of Climate,* 20, 5041–5060.
10. Greene, D. R. & Clark R. A. (1972). Vertically integrated liquid water-A new analysis tool. *Monthly Weather Review,* 100(7), 548-552.
11. Graham, N. & Barnett, T. (1987). Sea surface temperature, surface wind divergence, and convection over tropical oceans. *Science,* 238, 657–659.
12. Heymsfield, G. M., Tian, L., Heymsfield, A. J., Li, L. & Guimond, S. (2010). Characteristics of deep tropical and subtropical convection from nadir-viewing high-altitude airborne Doppler radar. *Journal of Atmospheric Science,* 67, 285–308.
13. Houze, R.A. (1982). Cloud clusters and large-scale vertical motions in the tropics. *Journal of Meteorological Society of Japan*, 60.
14. Houze, R. A. (1993). *Cloud Dynamics*. Academic Press, San Diego, 573 pp.
15. Houze, R. A. (1989). Observed structure of mesoscale convective systems and implications for large- scale heating. *Quarterly Journal of Royal Meteorological Society,* 115, 425-461.
16. Houze, R. A. & Betts, A. K. (1981). Convection in GATE. *Review of Geophysics Space Physics,* 19, 541-576.
17. Houze, R. A. & Cheng, C. P. (1977). Radar characteristics of tropical convection observed during GATE: Mean properties and trends over the summer season. *Monthly Weather Review.* 105, 964-980.
18. Houze, R. A., Wilton, D. C. & Smull, F. B. (2007). Monsoon convection in the Himalayan region as seen by the TRMM precipitation radar. *Quarterly Journal of Royal Meteorological Society,* 133, 1389–1411.
19. Imaoka, K. & Nakamura, K. (2012). Statistical analysis of the life cycle of isolated tropical cold cloud systems using MTSAT-1R and TRMM data. *Monthly Weather Review,* 140(11), 3552-3572.
20. Kalnay, E., Kanamitsu, M., Kistler, R., Collins, W., Deaven, D., Gandin, L., Iredell, M., Saha, S., White, G., Woollen, J. & Zhu, Y. (1996). The NCEP/NCAR 40-year reanalysis project. *Bulletin of American Meteorological Soc*iety, 77(3), 437-471.
21. Kumar, S. (2016). Three dimensional characteristics of precipitating cloud systems observed during Indian Summer monsoon. *Advance in Space Research*, *58*(6), 1017-1032.
22. Kumar, S. (2017a). A 10-year Climatology of Vertical Properties of Most Active Convective Clouds over the Indian Regions Using TRMM PR. *Theoretical and Applied Climatology,* 127 (1–2), 429–440.
23. Kumar, S. (2017b). Vertical Characteristics of Reflectivity in Intense Convective Clouds Using TRMM PR Data. *Environment and Natural Resources Research,* 7 (2), 58.
24. Kumar, S. (2018). Vertical Structure of Precipitating Shallow Echoes Observed from TRMM during Indian Summer Monsoon. *Theoretical and Applied Climatology,* 133 (3–4), 1051–1059.
25. Kumar, S. & Bhat, G. S. (2015). Vertical Structure of Radar Reflectivity in Deep Intense Convective Clouds over the Tropics. EGUGA 2302.
26. Kumar, S. & Bhat G. S. (2016). Vertical profiles of radar reflectivity factor in intense convective clouds in the tropics. *Journal of Applied Meteorological Climatol*ogy, *55*(5), 1277-1286.doi:10.1175/JAMC-D- 15-0110.1.
27. Kumar, S. & Bhat, G. S. (2017). Vertical Structure of Orographic Precipitating Clouds Observed over South Asia during Summer Monsoon Season. *Journal of Earth System Science,* 126 (8), 114.
28. Kumar, S. & Bhat, G. S. (2019). Frequency of a State of Cloud Systems over Tropical Warm Ocean. *Environmental Research Communications,* 1 (6), 061003.
29. Kumar, S., Silva, Y., Moya-Álvarez, A. S. & Martínez-Castro, D. (2019a). Seasonal and Regional Differences in Extreme Rainfall Events and Their Contribution to the World's Precipitation: GPM Observations. *Advances in Meteorology*, doi:10.1155/ 2019/4631609.
30. Kumar, S., Silva, Y., Moya-Álvarez, A. S. & Martínez-Castro, D. (2019b). Effect of the Surface Wind Flow and Topography on Precipitating Cloud Systems over the Andes and Associated Amazon Basin: GPM Observations. *Atmospheric Research,* 225 (193–208). doi:10.1016/ jAtmosres.2019.03.027.
31. Kumar, S., Castillo-Velarde, C. D., Flores Rojas, J. L., Moya-Alvarez, A. S., Martinez Castro, D., Srivastava, S. & Silva, Y. (2020a). Precipitation structure during various phases the life cycle of precipitating cloud systems using geostationary satellite and space-based precipitation radar over Peru. *GIScience & Remote Sensing*, 57(8), 1057-1082.
32. Shailendra, K., Moya-Álvarez, A. S., Castillo-Velarde, C.D., Martinez-Castro, D. & Silva, Y., (2020b). Effect of low-level low and Andes mountain on the tropical and mid-latitude precipitating cloud systems: GPM observations. *Theoretical and Applied Climatology,* 141 (1), 157–172.
33. Kumar, S., Castillo-Velarde, C. D., Valdivia Prado, J. M., Flores Rojas, J. L., Callañaupa Gutierrez, S. M., Moya Alvarez, A. S., Martine-Castro, D. & Silva, Y. (2020c). Rainfall Characteristics in the Mantaro-Basin over Tropical Andes from a Vertically Pointed Profiler Rain Radar and In -Situ Field Campaign. *Atmosphere,* 11 (3), 248.
34. Kumar, S. & Silva, Y. (2019). Vertical Characteristics of

Radar Reflectivity and DSD Parameters in Intense Convective Clouds over South East South Asia during the Indian Summer Monsoon: GPM Observations. *International Journal of Remote Sensing, 40*(24), 9604-9628.

35. Kumar, S. & Silva, Y. (2020). Distribution of Hydrometeors in Monsoonal Clouds over South American Continent during Austral Summer Monsoon: GPM Observations GPM Observations. *International Journal of Remote Sensing,* 41 (10), 3677–3707.
36. Kummerow, C., Barnes, W., Kozu, T., Shiue, J. & Simpson, J. (1998). The Tropical Rainfall Measuring Mission (TRMM) Sensor Package. *Journal of Atmospheric and Oceanic Technology*, 15, 809–817.
37. Kondo, Y., Higuchi, A. & Nakamura, K. (2006). Small-scale cloud activity over the Maritime Continent and the Western Pacific as revealed by satellite data. *Monthly Weather Review*, 134, 1581–1599.
38. Li, W. & Schumacher, C. (2011). Thick anvils as viewed by the TRMM precipitation radar. *Journal of Climate,* 24, 1718–1735.
39. Liu, G., & Fu, Y. (2001). The characteristics of tropical precipitation profiles as inferred from satellite radar measurements. *Journal of Meteorological Society Japan*, 79, 131–143.
40. Leary, C. A. & Houze, R. A. (1979). The structure and evolution of convection in a tropical cloud cluster. *Journal of Atmospheric Science,* 36, 437-457.
41. Machado, L. A. T., Rossow, W. B., Guedes, R. L. & Walker, A. W. (1998). Life cycle variations of mesoscale convective systems over the Americas. *Monthly Weather Rev*iew, 126, 1630–1654.
42. Mathon, V. & Laurent, H. (2001). Life cycle of Sahelian mesoscale convective cloud systems. *Quarterly Journal of Royal Meteorological Soc*iety, 127, 377–406.
43. Roca, R., Fiolleau, T. & Bouniol, D. (2017). A Simple model of the life cycle of mesoscale convective systems cloud shield in the tropics. *Journal of Climate*, 30 (11), 4283–4298.
44. Roca. R., Aublane, J., Chambon, P., Fiolleau, T. & Viltard, N. (2014). Robust Observational Quantification of the Contribution of Mesoscale Convective Systems to Rainfall in the Tropics. *Journal of Climate*, 27, 4952-4958. https://doi.org/10.1175/JCLI-D-13-00628.1
45. Schumacher, C. & Houze, R. A. (2000). Comparison of radar data from the TRMM satellite and Kwajalein oceanic validation site. *Journal of Applied Meteorology and Climatology*, *39*(12), 2151-2164.
46. Sherwood, S. C., Minnis, P. & McGill, M. (2004). Deep convective cloud-top heights and their thermodynamic control during crystal-face. *Journal of Geophysical, Research,* 109, doi:10.1029/2004JD004811.
47. Waliser, D. E. & Graham, N. E. (1993). Convective cloud systems and warm-pool sea surface temperatures: coupled interactions and self-regulation. *Journal of Geophysical Research Atmosphere*, 98, 12881–93.
48. Williams, E. R., Weber, M. E. & Orville, R. E. (1989). The relationship between lighting type and convective state of thunderstorms. *Journal of Geophysical Research Atmosphere,* 94,13213–13220.
49. Yuter, S. E. & Houze, R. A. (1995). Three-dimensional kinematic and microphysical evolution of Florida cumulonimbus: Part II. Frequency distribution of vertical velocity, reflectivity, and the differential reflectivity. *Monthly Weather Rev*iew, 123, 1941–1963.